Electronic Supplementary Material (ESI) for Dalton Transactions.
This journal is © The Royal Society of Chemistry 2021

Second Harmonic Generation on Chiral Cyanido-Bridged Fe^{II}-Nb^{IV} Spin Crossover Complexes

Shintaro Kawabata,[a] Koji Nakabayashi,[a]* Kenta Imoto,[a] Stephen Klimke,[b] Franz Renz,[b] and Shin-ichi Ohkoshi,[a]*

[a] Department *of Chemistry, School of Science, The University of Tokyo 7-3-1 Hongo, Bunkyo-ku, Tokyo 113-0033, Japan.*
[b] Institute of Inorganic Chemistry, Leibniz University Hannover, Callinstrasse 9, 30167 Hannover, Germany

*To whom correspondence should be addressed
E-mail: ohkoshi@chem.s.u-tokyo.ac.jp

Table of Contents:

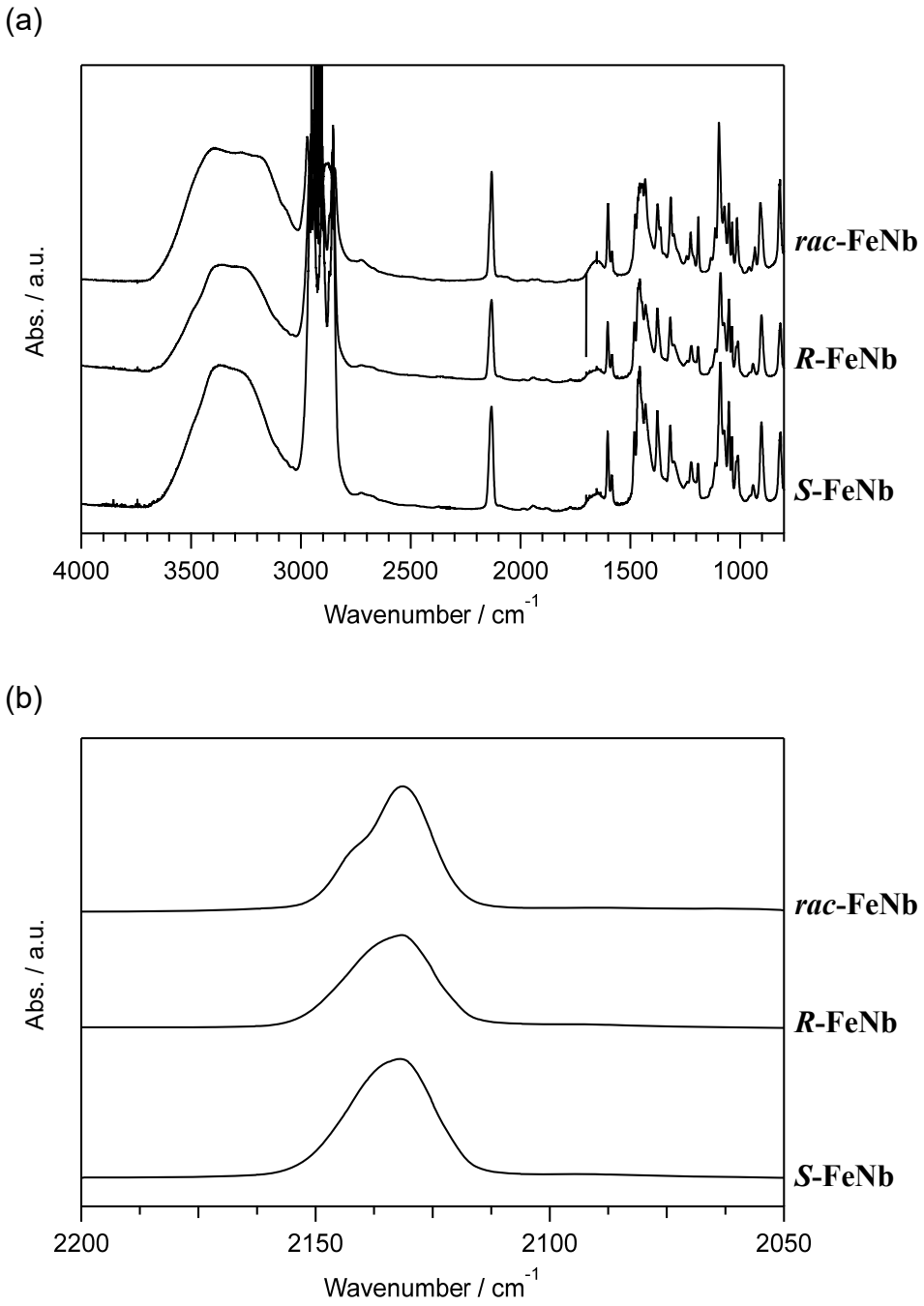

Figure S1. IR spectra of ***rac*-FeNb**, ***R*-FeNb**, and ***S*-FeNb** in the whole range (a) and in the range related to the CN^- stretching vibrations (b) at room temperature.

***rac*-FeNb**

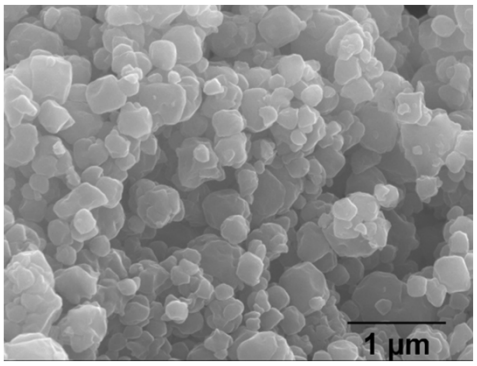

***R*-FeNb**

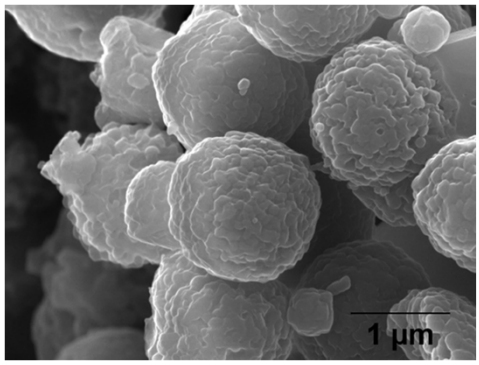

***S*-FeNb**

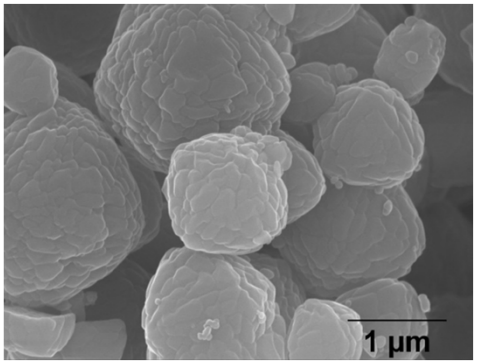

Figure S2. SEM images of ***rac*-FeNb**, ***R*-FeNb**, and ***S*-FeNb**.

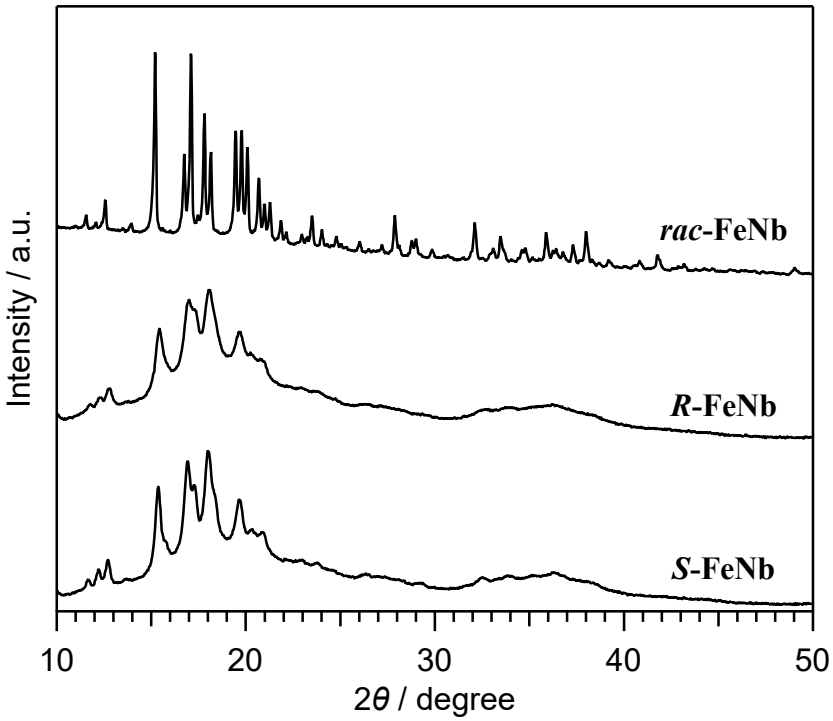

Figure S3. PXRD patterns of ***rac*-FeNb**, ***R*-FeNb**, and ***S*-FeNb** at room temperature.

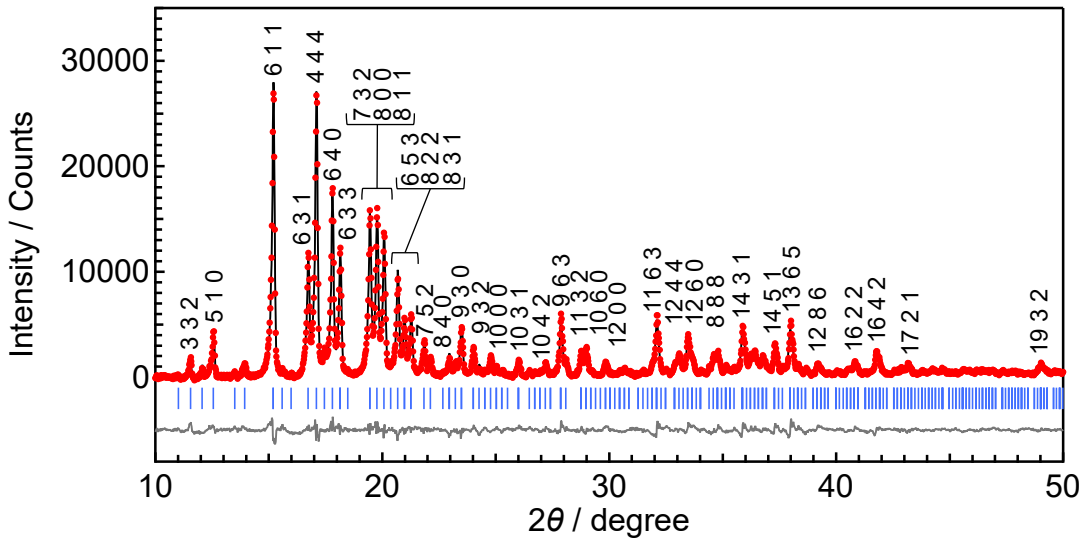

Figure S4. PXRD pattern and the result of Rietveld analysis for ***rac*-FeNb** at room temperature. Red dots, black line, blue bar, and gray line represent the experimental data, the calculated pattern, Bragg diffractions of the target compound, and residual curve, respectively.

Table S1. Crystallographic data from Rietveld analyses of the PXRD patterns of ***rac*-FeNb** at room temperature.

Crystal system	Cubic
Space group	$Ia\bar{3}d$
a / Å	35.8996(5)
Z	24
V/ Å^3	46255
d/ g cm^{-3}	1.30
R_{wp}/ R_p	0.0214/ 0.0164
S	1.97
T/ K	294

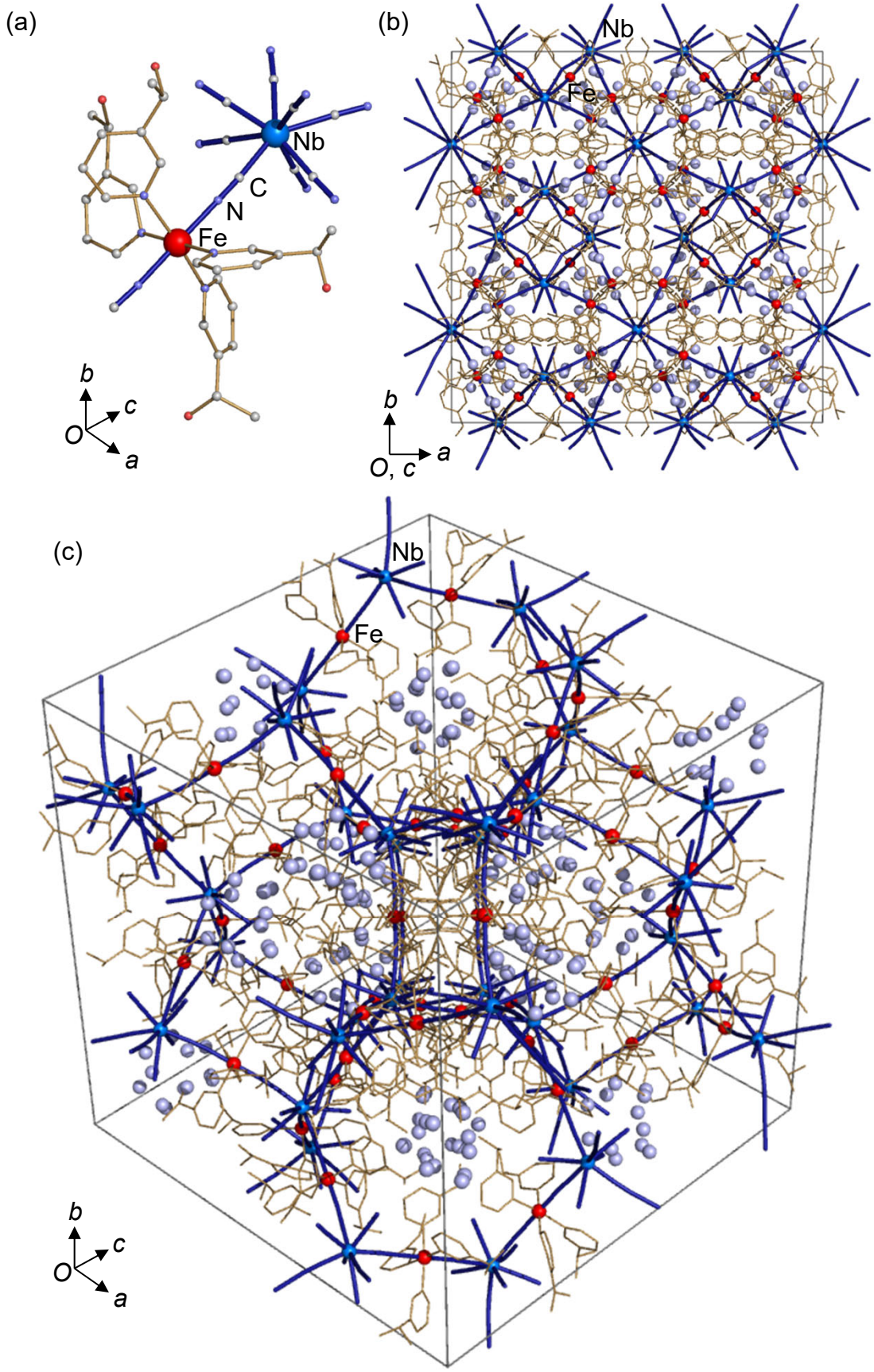

Figure S5. Crystal structure of ***rac*-FeNb**. (a) Coordination geometry. (b) View from the *c* axis. (c) View from the [111] direction. Red, blue, and light blue spheres show Fe, Nb, and O (water molecule) atoms, respectively. Light brown, blue thick line, and gray lines represent 1-(3-pyridyl)ethanol, 3-D cyanido-bridged coordination network, and the unite cell, respectively.

Table S2. Subgroups of $Ia\bar{3}d$ in cubic system. The numbers in parentheses are respective space group numbers.

	$I\bar{4}3d$ (220)	
$Ia\bar{3}d$ (230)	$I4_132$ (214)	**$I2_13$ (199)**
	$Ia\bar{3}$ (206)	

black: centrosymmetric; brown: non-centrosymmetric, achiral
red: non-centrosymmetric, chiral
blue: non-centrosymmetric, chiral but SHG inactive

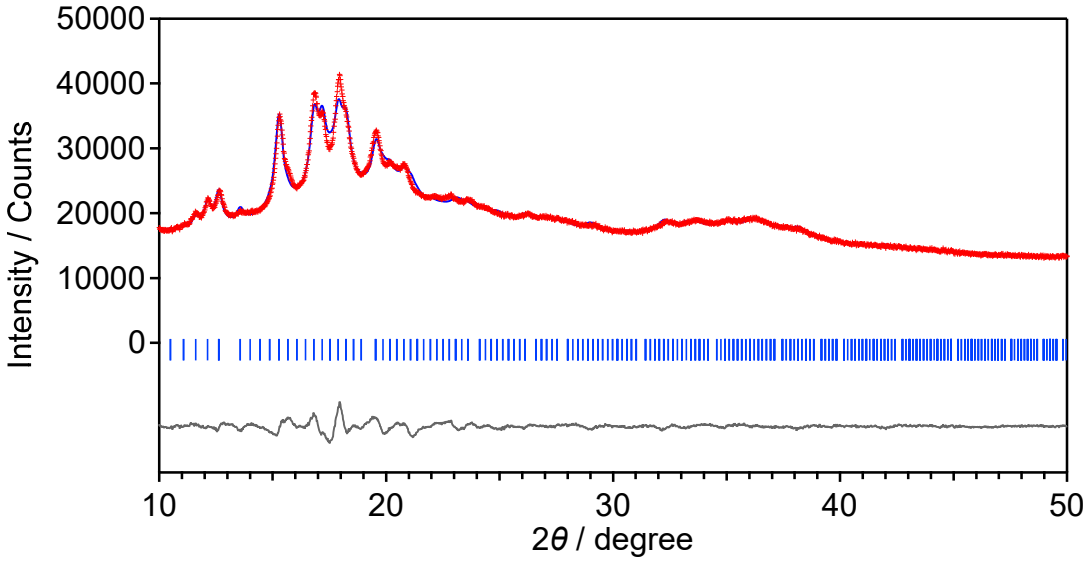

Compound	***R*-FeNb**
Crystal system	Cubic
Space group	$I2_13$
a / Å	35.753(3)
R_{wp} / R_p	0.0196 / 0.0135
S	2.67

Figure S6. Rietveld analysis of the PXRD patterns of ***R*-FeNb** at room temperature.

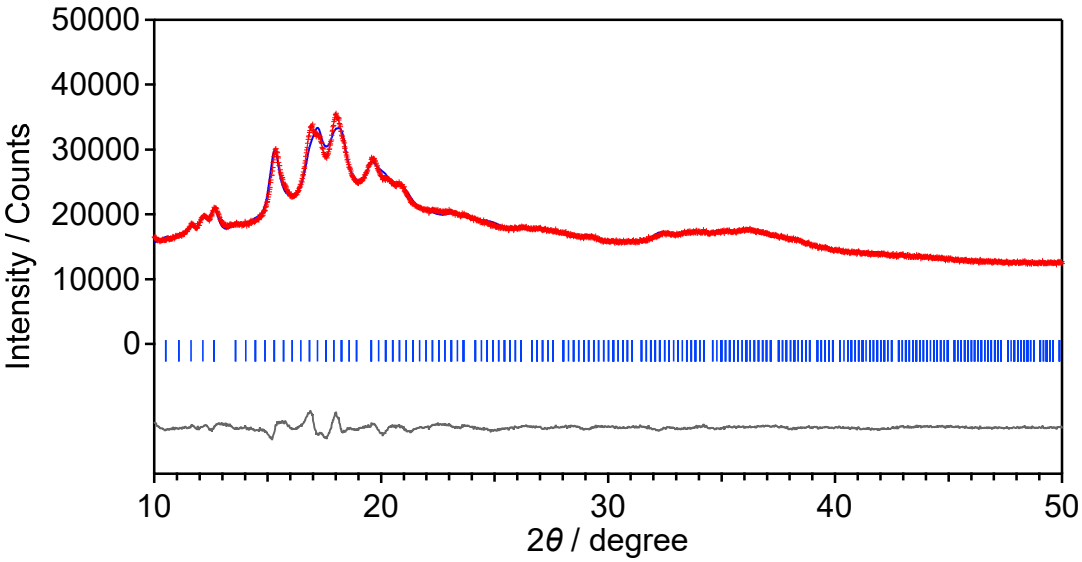

Compound	***S*-FeNb**
Crystal family	Cubic
Space group	$I2_13$
a / Å	35.709(4)
R_{wp} / R_p	0.0178 / 0.0127
S	2.32

Figure S7. Rietveld analysis of the PXRD patterns of ***S*-FeNb** at room temperature.

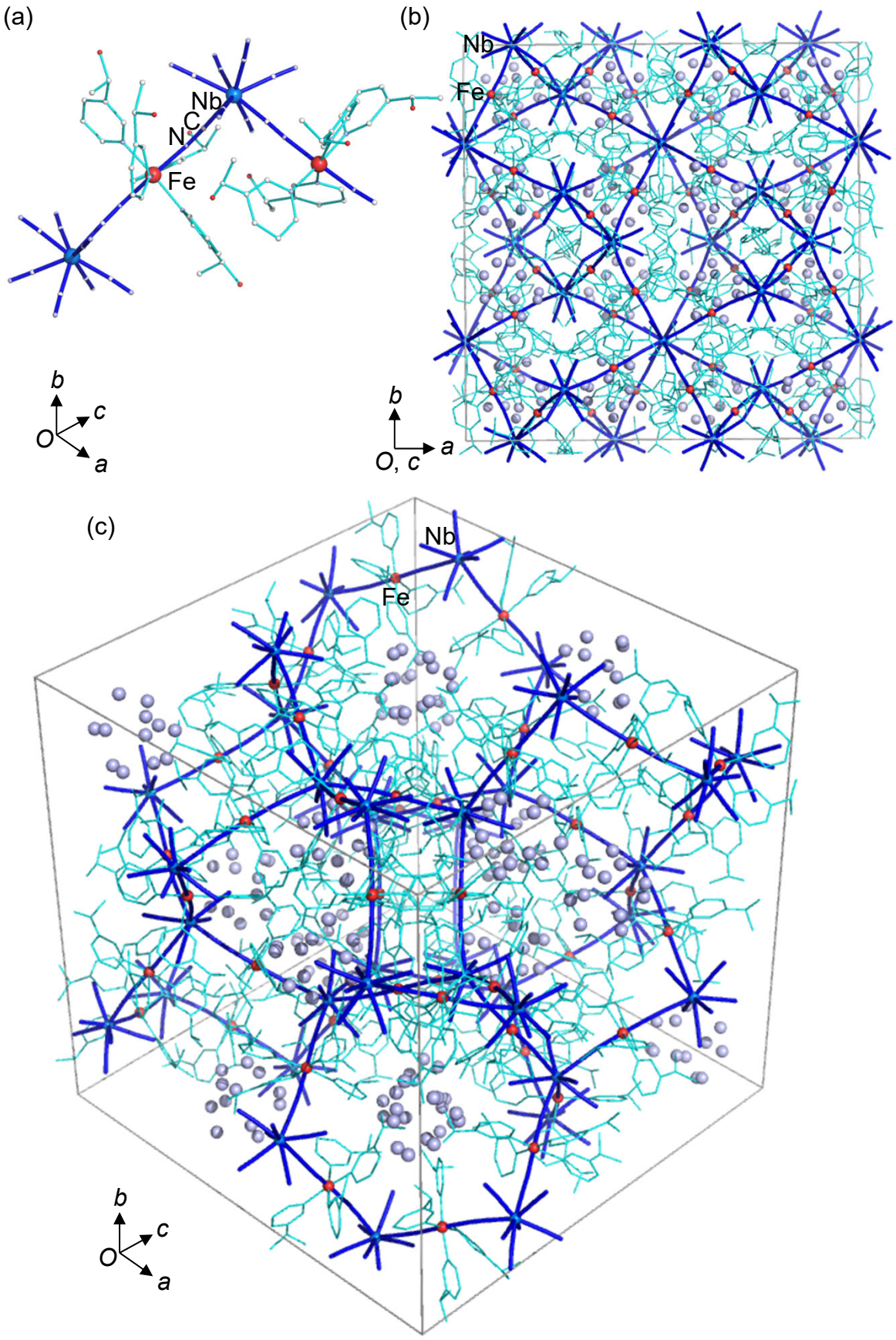

Figure S8. The structure based on the Rietveld analysis for ***S*-FeNb**. (a) Coordination structure around Fe and Nb. (b) View from the *c* axis. (c) View from the [111] direction. Red, blue, and light blue spheres show Fe, Nb, and O (water molecule) atoms, respectively. Light pink, blue thick, and gray lines represent *S*-1-(3-pyridyl)ethanol, 3-D cyanido-bridged coordination network, and the unite cell, respectively.

Table S3. Bond lengths (Å) between Fe-N atoms obtained the Rietveld analyses of the PXRD patterns of ***R*-FeNb** and ***S*-FeNb** at room temperature.

T/ K	***R*-FeNb**	***S*-FeNb**
Fe1-N1	2.20(3)	2.17(2)
Fe1-N6	2.09(3)	2.123(18)
Fe1-N9	2.207(16)	2.217(14)
Fe1-N10	2.234(15)	2.222(12)
Fe1-N11	2.198(16)	2.138(14)
Fe1-N12	2.087(13)	2.133(11)
Average of Fe1-N	**2.17(2)**	**2.167(15)**
Fe2-N2	2.13(2)	2.136(18)
Fe2-N3	2.16(2)	2.135(18)
Fe2-N13	2.175(16)	2.183(14)
Fe2-N14	2.223(15)	2.137(12)
Fe2-N15	2.150(15)	2.227(13)
Fe2-N16	2.088(13)	2.176(10)
Average of Fe2-N	**2.154(17)**	**2.166(14)**

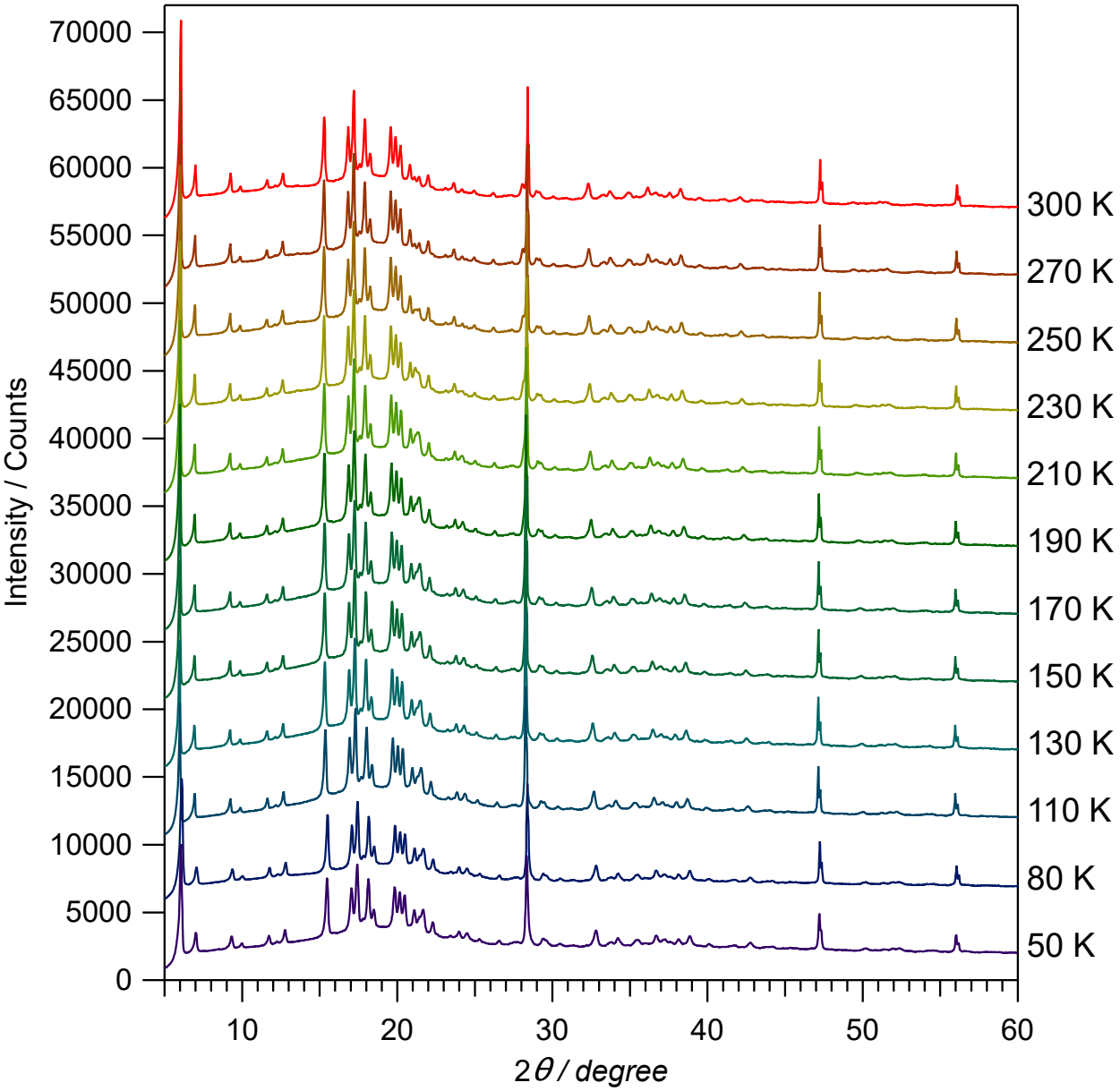

Figure S9. Variable-temperature PXRD patterns of ***rac*-FeNb** at respective temperatures. The sharp peaks at 28° , 47° , and 56° represent the diffractions from the Si used for the calibration of temperature shift of the pattern in the applied measurement system.

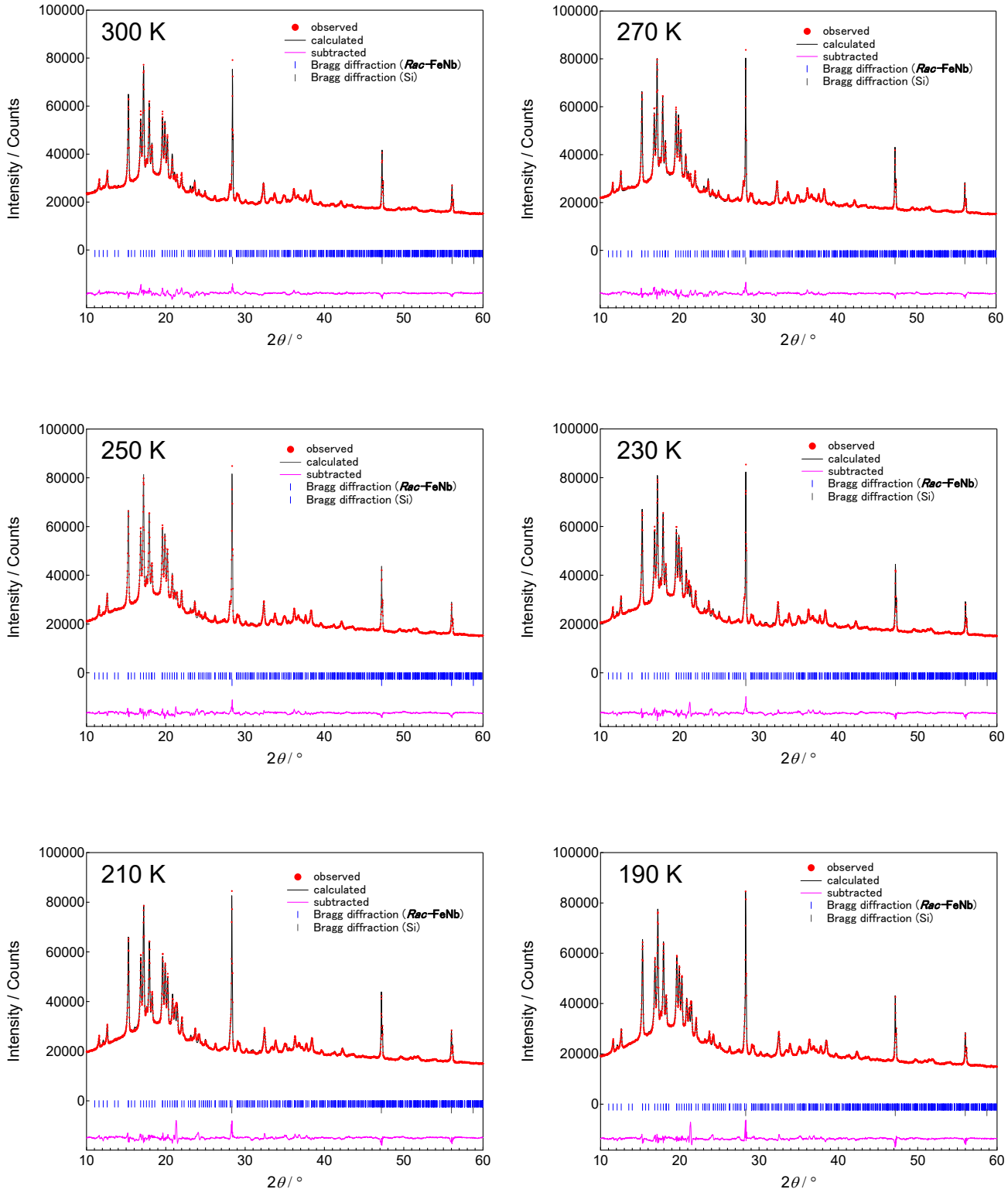

Figure S10. Rietveld analyses of the PXRD patterns of ***rac*-FeNb** at respective temperatures.

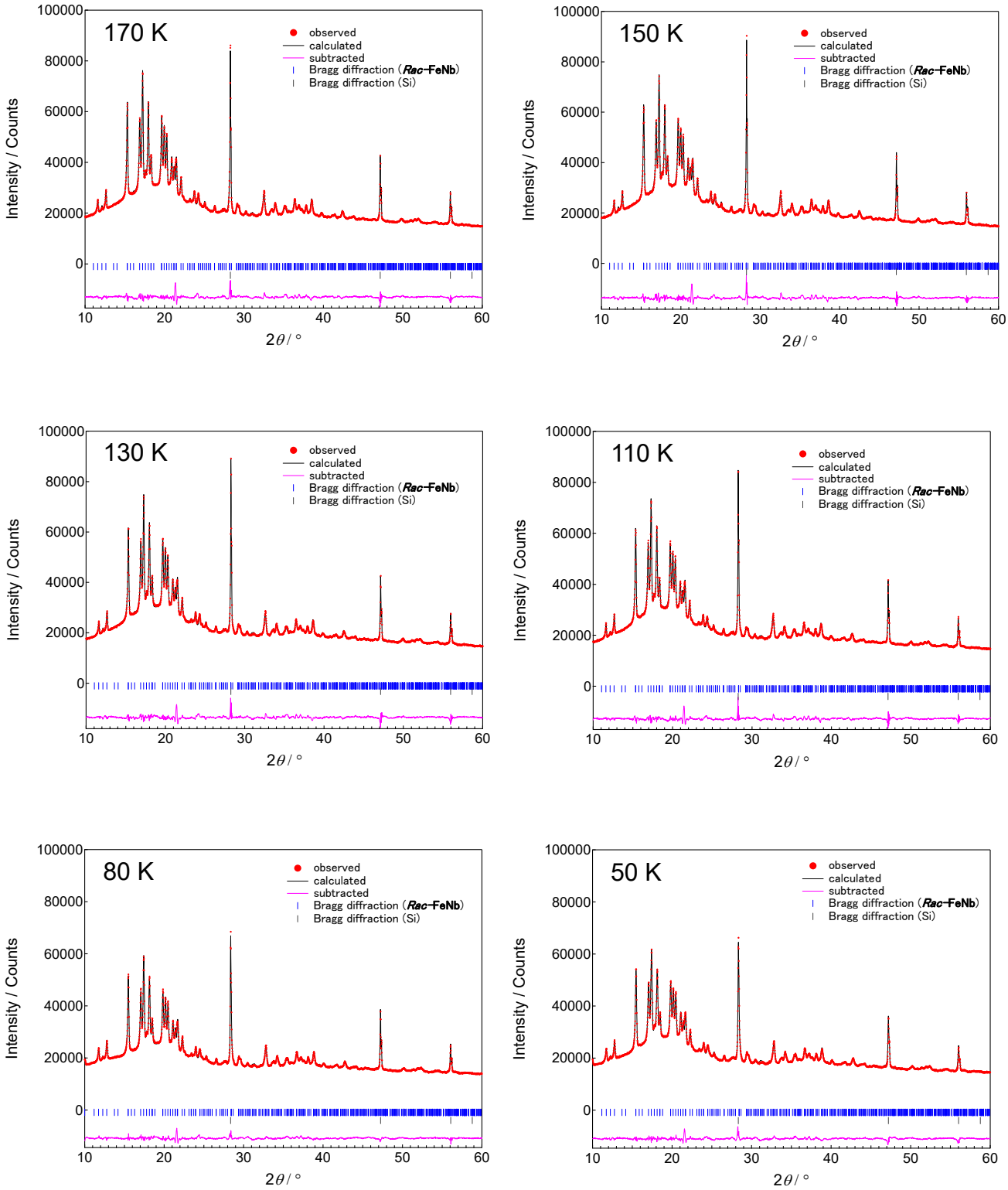

Figure S10 (Continued)**.** Rietveld analyses of the PXRD patterns of ***rac*-FeNb** at respective temperatures.

Table S4. Crystallographic data from Rietveld analyses of the PXRD patterns of ***rac*-FeNb** at respective temperatures.

T / K	300(2)	270(2)	250(2)	230(2)	210(2)	190(2)
Space group	$Ia\bar{3}d$					
a / Å	35.645(2)	35.592(2)	35.548(2)	35.493(2)	35.432(2)	35.361(2)
V /Å^3	45291(3)	45084(3)	44918(3)	44711(4)	44483(4)	44217(3)
d / g cm^{-3}	1.33	1.33	1.34	1.34	1.35	1.36
S	2.79	2.64	2.66	3.18	3.47	3.30
Z	24					
R_p	0.0136	0.0133	0.0130	0.0152	0.0152	0.0154
R_{wp}	0.0185	0.0175	0.0176	0.0210	0.0230	0.0219

T / K	170(2)	150(2)	130(2)	110(2)	80(2)	50(2)
Space group	$Ia\bar{3}d$					
a / Å	35.295(2)	35.239(1)	35.2004(9)	35.134(1)	35.091(2)	35.048(2)
V /Å^3	43968(4)	43758(4)	43616(2)	43368(3)	43211(3)	43051(4)
d / g cm^{-3}	1.37	1.37	1.38	1.38	1.39	1.39
S	3.42	3.11	3.13	2.92	2.38	2.58
Z	24					
R_p	0.0136	0.0137	0.0143	0.0133	0.0121	0.0121
R_{wp}	0.0207	0.0208	0.0210	0.0197	0.0170	0.0178

Table S5. Bond lengths (Å) between Fe-N atoms obtained the Rietveld analyses of the PXRD patterns of ***rac*-FeNb** at respective temperatures.

T/ K	300	270	250	230	210	190
Fe-N1	2.139	2.147	2.151	2.146	2.133	2.121
Fe-N3	2.166	2.148	2.139	2.136	2.135	2.129
Fe-N4	2.192	2.190	2.200	2.194	2.190	2.186
Fe-N5	2.187	2.179	2.149	2.140	2.097	2.088
Average of Fe1-N	**2.165**	**2.160**	**2.155**	**2.150**	**2.137**	**2.129**
T/ K	170	150	130	110	80	50
Fe-N1	2.102	2.084	2.080	2.065	2.063	2.053
Fe-N3	2.131	2.131	2.125	2.126	2.110	2.112
Fe-N4	2.175	2.171	2.170	2.154	2.107	2.096
Fe-N5	2.086	2.072	2.068	2.061	2.052	2.040
Average of Fe-N	**2.121**	**2.112**	**2.108**	**2.099**	**2.084**	**2.078**

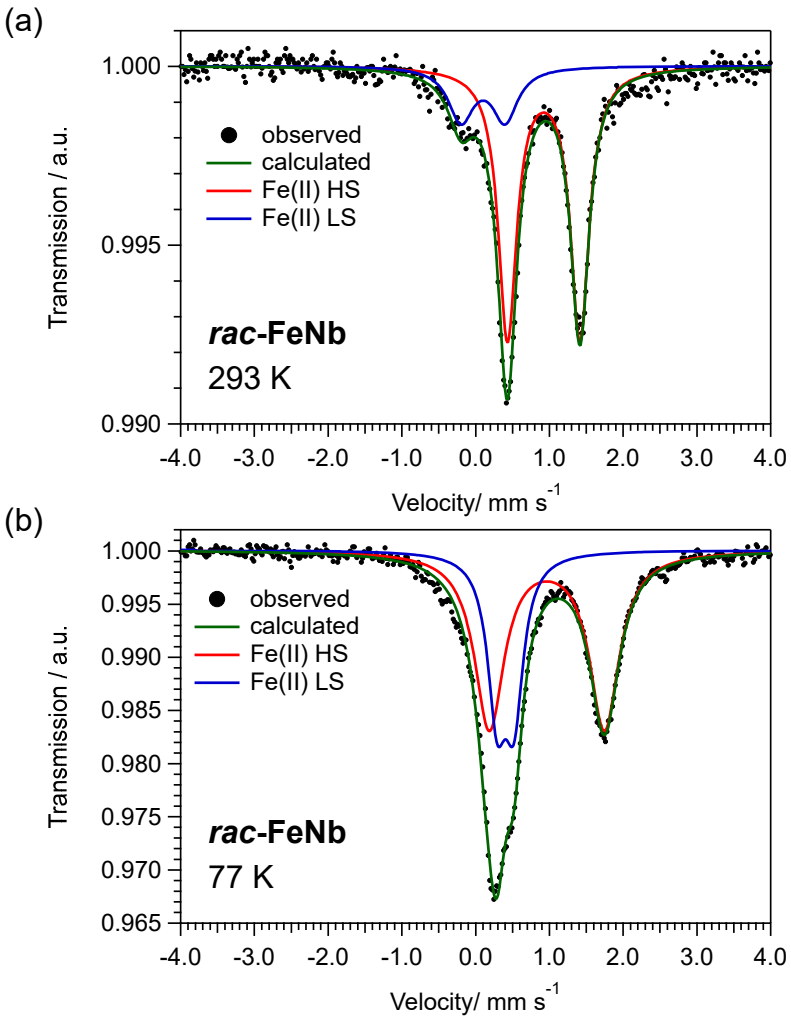

Figure S11. ^{57}Fe Mössbauer spectra of ***rac*-FeNb** at 293 K (a) and 77 K (b). Black dots represent observed data. Green line shows the total calculated curve deconvoluted into the Fe^{II}_{HS} doublets (Red and orange lines) and the Fe^{II}_{LS} doublet (blue line).

Table S6. ^{57}Fe Mössbauer spectra parameters for ***rac*-FeNb**.

Compound	T (K)	Assignment of Fe sites	δ (mm s^{-1})	ΔE_Q (mm s^{-1})	Γ (mm s^{-1})	Fraction (%)
***rac*-FeNb**	293	Fe^{II}_{HS} (doublet 1)	1.03(1)	0.98(2)	0.15(1)	79
		Fe^{II}_{LS} (doublet 2)	0.21(6)	0.6(1)	0.21(4)	21
	77	Fe^{II}_{HS} (doublet 1)	1.07(1)	1.56(1)	0.24 (1)	65
		Fe^{II}_{LS} (doublet 2)	0.51(1)	0.23(1)	0.15(1)	35

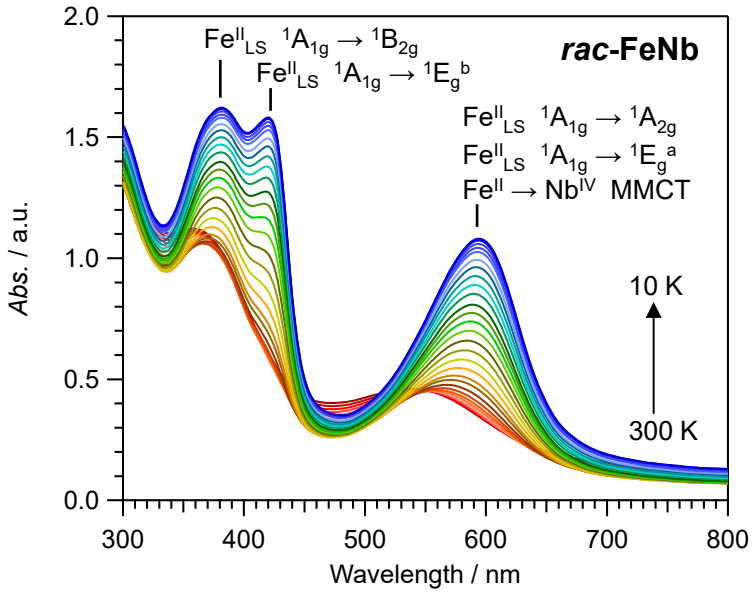

Figure S12. Variable-temperature solid-state UV–vis absorption spectra of ***rac*-FeNb** from 300 K to 10 K.

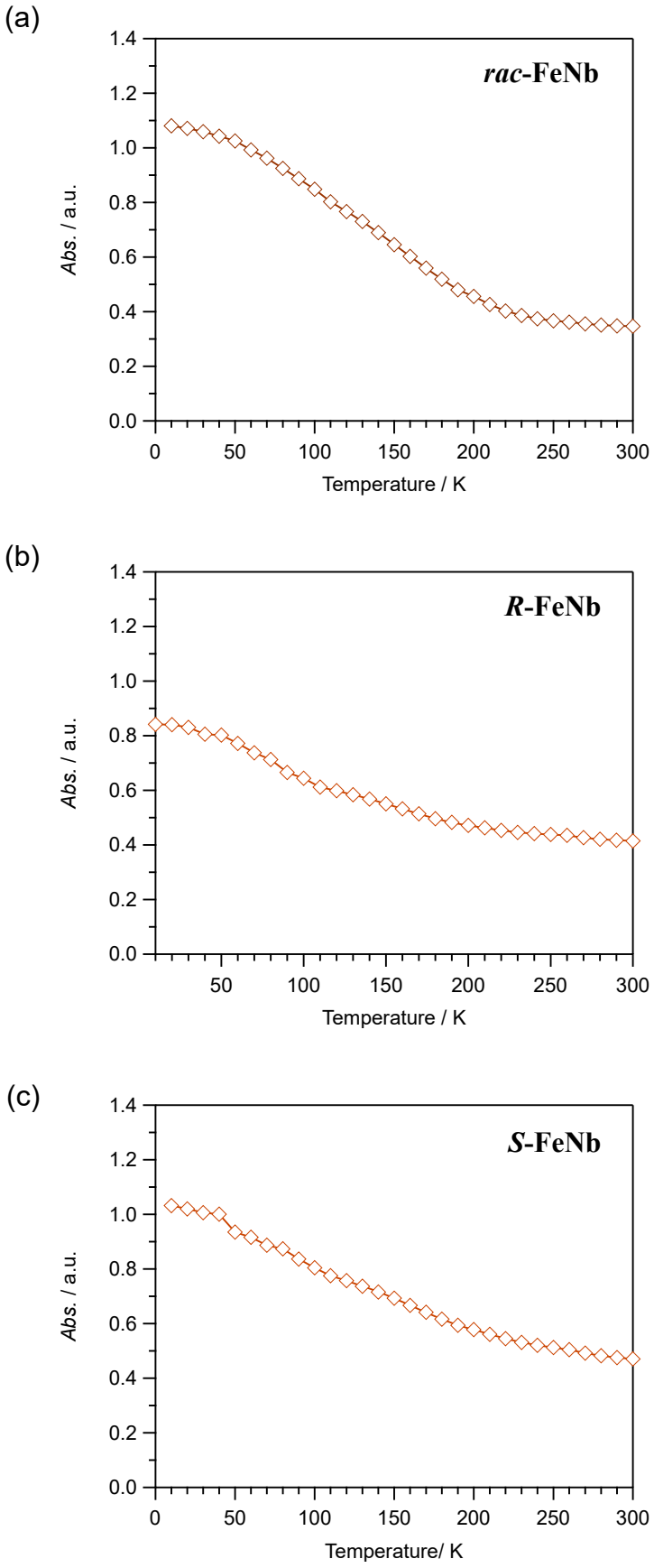

Figure S13. Temperature dependences of the absorbances at 595 nm in the solid-state UV–vis absorption spectra of ***rac*-FeNb**, ***R*-FeNb** and ***S*-FeNb**.

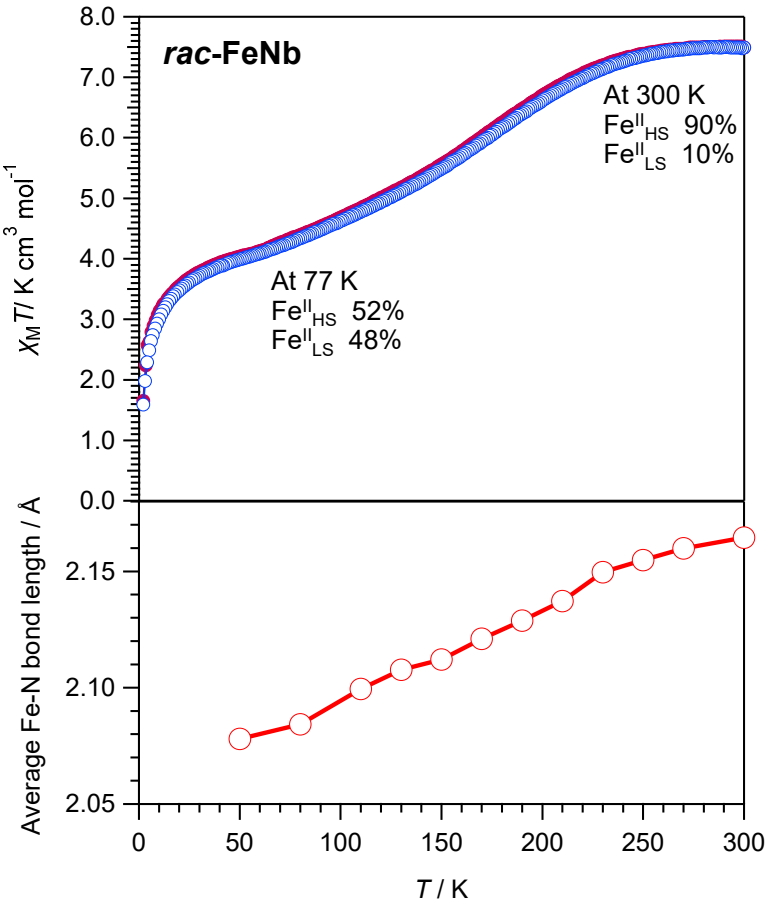

Figure S14. The $\chi_M T$ vs T plot product of ***rac*-FeNb** under 5000 Oe. Blue open and red circles indicate the cooling and heating processes, respectively (top). Temperature-dependence of the average Fe-N bond length in the crystal structure of ***rac*-FeNb** (bottom).

The $\chi_M T$–T plot above 290 K and from 10 to 50 K are analyzed based on the following Hamiltonian,

$$H = \kappa\lambda \boldsymbol{L} \cdot \boldsymbol{S} + \Delta\left({L_z}^2 - \frac{2}{3}\right)$$

where κ, λ, and Δ are orbital reduction factor, spin-orbit coupling parameter, and axial splitting parameters, respectively. The molar magnetic susceptibility (χ_M) is obtained by Van-Vleck equation.[S3] Furthermore, superexchange interaction between Fe and Nb is included by applying the molecular field theory based on the following spin Hamiltonian,

$$H = -JS_{Fe}S_{Nb}$$

The $\chi_M T$ value from 10 to 50 K is analyzed by multiplying high spin fraction (f_{HS}) to the calculated $\chi_M T$ value of high temperature region.

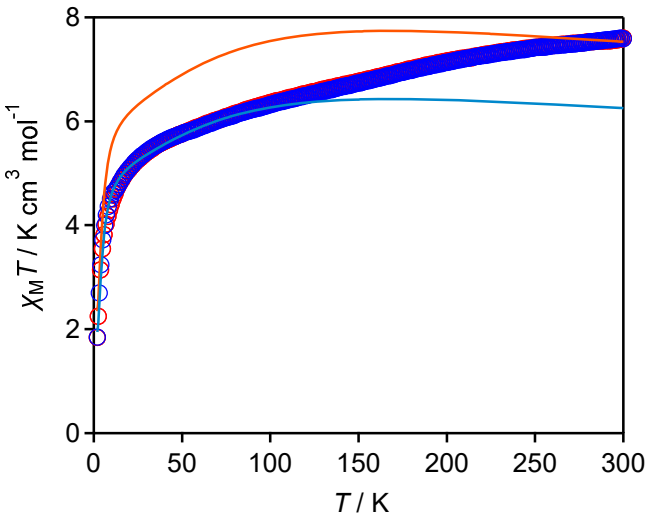

Figure S15. Magnetic analysis for the $\chi_M T$–T plot of ***R*-FeNb**. Red and blue plots are $\chi_M T$ values in the cooling and warming processes, respectively. The $\chi_M T$–T plot above 290 K is reproduced by using parameters, κ = 1, λ = −100 cm^{-1}, Δ = 105 cm^{-1}, J = −0.44 cm^{-1}, and f_{HS} = 0.91 (orange line). The plot in the range from 10 to 50 K is reproduced by using f_{HS} = 0.76 and the same parameters of κ, λ, and Δ as above 290 K (light blue line).

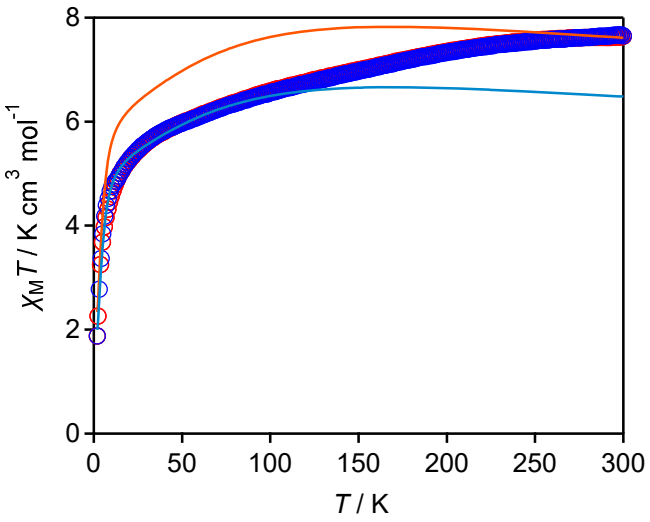

Figure S16. Magnetic analysis for the $\chi_M T$–T plot of ***S*-FeNb**. Red and blue plots are $\chi_M T$ values in the cooling and warming processes, respectively. The $\chi_M T$–T plot above 290 K is reproduced by using parameters, $\kappa = 1$, $\lambda = -100$ cm^{-1}, $\Delta = 106$ cm^{-1}, $J = -0.44$ cm^{-1}, and $f_{HS} = 0.92$ (orange line). The plot in the range from 10 to 50 K is reproduced by using $f_{HS} = 0.78$ and the same parameters of κ, λ, and Δ as above 290 K (light blue line).

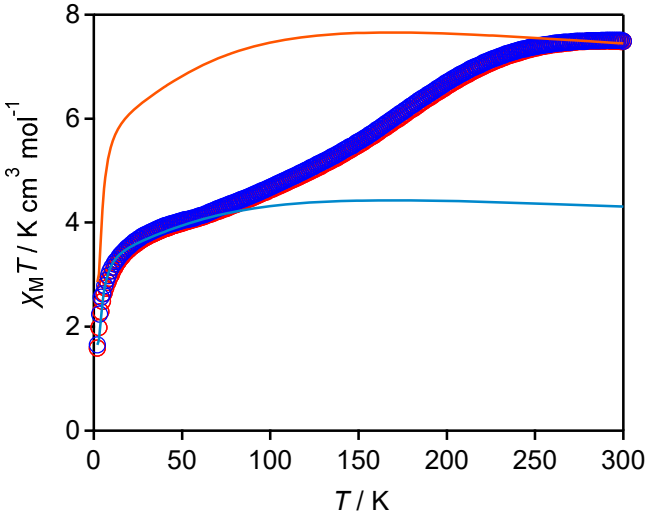

Figure S17. Magnetic analysis for the $\chi_M T$–T plot of ***rac*-FeNb**. Red and blue plots are $\chi_M T$ values in the cooling and warming processes, respectively. The $\chi_M T$–T plot above 290 K is reproduced by using parameters, $\kappa = 1$, $\lambda = -100$ cm^{-1}, $\Delta = 97$ cm^{-1}, $J = -0.48$ cm^{-1}, and $f_{HS} = 0.90$ (orange line). The plot in the range from 10 to 50 K is reproduced by using $f_{HS} = 0.52$ and the same parameters of κ, λ, and Δ as above 290 K (light blue line).

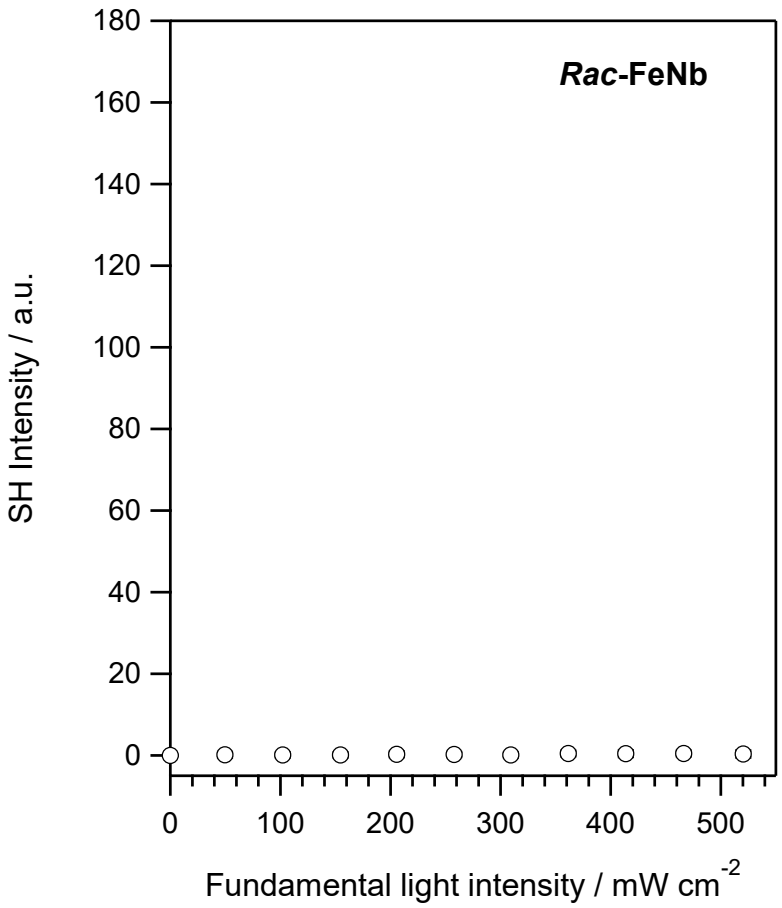

Figure S18. SH intensity vs incident light power (1040 nm) plot of ***rac*-FeNb** at 293 K.